On the Interfacial Behavior of Catenated Poly(L-Lactide) at Air-Water Interface

Li-Han Rong[1], Xiang Cheng[1], Jin Ge[1], Hanyu Wang[2], Peng-Fei Cao[3], Eugene B. Caldona[4], and Rigoberto C. Advincula[1,2,4]**

[1]Department of Macromolecular Science and Engineering, Case Western Reserve University, Cleveland, OH 44106, United States

[2]Center for Nanophase Materials Sciences (CNMS), Oak Ridge National Laboratory, Oak Ridge, TN 37830, United States

[3]Chemical Sciences Division, Oak Ridge National Laboratory, Oak Ridge, TN 37830, United States

[4]Department of Chemical and Biomolecular Engineering and Institute for Advanced Materials and Manufacturing, University of Tennessee, Knoxville, TN 37996, United States

Corresponding Authors [*]: Prof. R. C. Advincula (rca41@case.edu) and Peng-Fei Cao (caop@ornl.gov).

KEYWORDS: catenated polymer, air-water interface, Langmuir-Blodgett film

ABSTRACT

Interfacial properties of polymeric materials are significantly influenced by their architectural structures and spatial features. In this work, we studied, for the first time, the interfacial behavior of catenated poly(L-lactide) (C-PLA) at the air-water interface and compared it with its linear alternative (L-PLA). Results from the surface pressure-area per repeating unit isotherms showed significant interfacial behavioral difference between the two polymers. Isobaric creep experiments and compression-expansion cycles also showed that C-PLA demonstrated higher stability at the air-water interface. Furthermore, when the films at different surface pressures were transferred via the Langmuir-Blodgett method, successive atomic force microscopy imaging displayed distinct nanomorphologies, in which the surface of C-PLA exhibited nanofibrous structures, while that of the L-PLA revealed a smoother topology with fewer fiber-like structures.

INTRODUCTION

Topological structures have been proven effective in determining the air-water interfacial behavior of many polymeric materials.[1] Topological polymers exhibit more unique self-assembling morphology[2-3] and distinctive interfacial properties,[4-5] compared to their linear alternatives. Considered as one of the most commonly used methods for interfacial studies, the Langmuir-Blodgett (LB) film technique renders well-controlled dynamic studies and efficiently transfers well-ordered monolayers to solid substrates.[6-8] A wide range of techniques, including atomic transfer microscopy (AFM),[9] transmission electron microscopy (TEM),[10] Brewster angle microscopy (BAM),[11] and X-ray diffraction (XRD),[12-13]can be used in tandem with LB to investigate the self-assembly and crystallinity of polymers with different topological structures. For example, Leon et al.[14] synthesized dendronized polymers with varying degrees of polymerization and found that high generation of dendrons showed stronger intermolecular interaction at the air-water interface and formed more ordered monolayers via LB technique. Using different ratios of hydrophobic to hydrophilic blocks, Patrick et al.[15] synthesized a series of copolymers that exhibited distinguishing morphologies and stability when transferred to a solid substrate and examined by AFM. Polylactide (PLA), a biocompatible and biodegradable polymer, has received significant attention, not only because of its practical applications in thin film coatings, drug delivery, and tissue engineering,[16-17] but also due to the interesting air-water interfacial behavior of its stereocomplex and topological analogues.[18-19] For example Kenta et al.[20] used LB technique in conjunction with AFM to investigate the surface morphology, crystallinity, and distinctive behavioral response during isothermal compression of linear and cyclic PLA stereocopolymers.

While much work has been done on investigating the interfacial properties of branched polymers,[21-22] the interfacial behavior of block copolymers,[23-24] cyclic polymers,[25-27] and high-order topological polymers, such as catenanes, knots, and rotaxanes, at the air-water interface has been rarely studied due to the difficulty in their synthesis.[28-29] Although some studies have explored catenated molecules using entropic driving ring-closure method,[30-31] this statistical-based approach requires a highly dilute condition to minimize the intermolecular reactions, which, in turn, reduce the yield of these polymers and, thus, limit their characterization. Previously, our group designed a rational strategy for synthesizing catenated poly(L-lactide) (C-PLA) in bulk.[32-33] The high yield and substantial amount of C-PLA that we synthesized allowed us to investigate the interfacial behavior of highly ordered polymeric structures.

In this study, we investigated the interfacial behavior of C-PLA at the air-water interface and compared the result with its linear alternative (L-PLA). To the best of our knowledge, the behavior of catenated polymeric materials at the air-water interface has not been reported. To address the behavioral and stability difference between these two polymers caused by their architectural structures, isothermal compression, isobaric creep, and compression-expansion hysteresis cycle experiments were employed. Furthermore, the films formed at different surface pressures were transferred to solid substrates for AFM imaging.

EXPERIMENTAL SECTION

Materials. L-PLA, C-PLA, and decomplex-catenated poly(L-lactide) (DC-PLA) were synthesized following the procedures recently reported by our group (Supporting Information (SI), Scheme S1) [reference]. HPLC grade chloroform, used to dissolve the polymers, was purchased from Fisher Scientific and used as received. Milli-Q water (18.2 MΩ cm resistivity) was used in all experimental procedures where the use of water was required.

Langmuir-Blodgett Studies. A KSV-2000 system (KSV Instruments, Finland) equipped with a standard trough (width = 150 mm and area = 78000 mm^2) was used to investigate the monolayer interfacial properties and stability of the catenated and knotty polymers. The trough was cleaned with ethanol prior to filing with water. 25 μL of each polymer was dissolved in chloroform, giving a solution concentration of 2.0 mg mL^{-1}, where 10 drops of each were spread carefully on the water surface. The solution was allowed to evaporate from the water for 15 min prior to conducting any experiments. The π-A isotherms and compression-expansion tests were measured at a constant compression or release rate of 10 mm min^{-1}.

AFM experiment. The interfacial structure of the polymer films was characterized by first transferring the floating layer onto silica wafer substrates, which were cleaned by sonication in acetone and successive plasma for 2 min prior to coating. The silica wafers were also immersed in the subphase before spreading the solution. After 15 min of chloroform evaporation, the barrier compressed according to the desired surface pressure and the substrates were pulled from the interface at a rate of 1 mm min^{-1}. AFM was then performed on a Park System NX-10 atomic force microscope using the tapping mode.

X-ray reflectivity measurement. To gain insights on the structural profile of the LB thin films, X-ray reflectivity was performed on a Rigaku SmartLab X-ray diffractometer equipped with a PhotonMax high-flux 9-kW rotating anode and Cu-Kα radiation having a wavelength of 1.54 Å. The sample was aligned and measured on a motorized adjustable Rx-Ry sample stage capable of properly positioning the sample along the x-y direction, and commonly used for precise correction of substrate/film mis-cut for perfect on-axis measurement. Both the incidence and detector slit had a width of 2.5°. The reflectivity measurement was performed at incidence angles of 0 to 10° using

a 0.01° increment and rate of 0.666° per min. The film thickness, density, and roughness profiles were constructed using an Igor Pro 8.04 with a motofit add-on by Andrew Nelson [1].

Other characterizations. Electrochemical impedance spectroscopy (EIS) was performed using a XX potentiostat/galvanostat (COMPANY) from XX kHz to XX Hz at a 10-mV AC voltage about the open-circuit potential, with Ag/AgCl, Pt, and polymer coated on gold-coated glass substrates as the reference, counter, and working electrodes, respectively. Differential scanning calorimetry (DSC) was done using a DSC XXX (COMPANY) at a ramp rate of XX °C min^{-1} and N_2 purge rate of XX °C min^{-1}.

RESULTS AND DISCUSSION

The structural design and synthesis of both C-PLA and L-PLA (Scheme 1) have been previously reported by our group.[33] As shown in Scheme S1 in the Supporting Information (SI), a templated catenane initiator was first prepared by complexing a triethylene glycol functionalized phenanthroline with copper and subsequent ring closure with dibutyldimethoxytin. C-PLA was then synthesized by inserting L-lactide monomer without breaking the catenane structure. For comparison, decomplexed PLA (DC-PLA) was prepared by removing the copper using KCN. Meanwhile, L-PLA was synthesized from L-lactide monomer using the same tin initiator. To obtain comparable results, the molecular weight of each ring in the C-PLA structure was kept nearly similar to that of L-PLA. Details on the molecular weight of these polymers are shown in Table S1.

Scheme 1

Surface Pressure-Area Isotherms. Figure 1 shows the surface pressure-area per repeating unit (π -A) isothermal compression curves for both L-PLA and C-PLA at 20 °C. Note that the area per

repeating unit is calculated from the polymer concentration, total spread volume, and degree of polymerization (see section 2 of the SI for more details on the calculation). Consistent with the previous report,[18] three different regions can be observed on the L-PLA isotherm: (i) a low surface pressure liquid-expansion region as evidenced by a sharp knee feature; (ii) a plateau attributed to the 2D chain to helix conversion or double layer formation;[34] and (iii) a low compressible, high surface pressure region due to a multilayer formation.[18] C-PLA also exhibited a similar three-region behavior, but with different values of area and surface pressure. The transition from liquid-expansion to the plateau region for C-PLA occurred at 7.2 mN m^{-1} surface pressure, higher than that of the L-PLA (4.8 mN m^{-1}), while the corresponding area per repeating unit for C-PLA (24.8 $Å^2$) was lower than L-PLA (29.4 $Å^2$). This result indicates that C-PLA forms a more compact self-assembly structure than L-PLA. This phenomenon can also be evidenced by the transition of the plateau region to the high surface pressure zone, where a higher transition surface pressure of 9.7 mN m^{-1} for C-PLA can be observed, compared to a value of 6.8 mN m^{-1} for L-PLA, coupled with a change in area per repeating unit from 13.9 $Å^2$ for L-PLA to 9.2 $Å^2$ for C-PLA. As shown in Figure S1, following decomplexation (i.e. removing the copper), the resulting DC-PLA isotherm showed no significant difference from that of C-PLA, implying that the self-assembly behavior of C-PLA is unaffected after decomplexation.

Figure 1

To compare the elasticity of both L-PLA and C-PLA, the compressibility, C, and compressional elasticity, ε_s, were determined from the isotherm curves using the following equation:[34]

$$\varepsilon_s = C^{-1} = -A\left(\frac{\partial \pi}{\partial A}\right)_T$$

where A is the area per repeating unit, π refers to the surface pressure, and T is the temperature (which is kept constant). The calculated results are plotted in Figure S2. At the beginning of compression, the polymers started to touch each other. Preliminary compression showed that both polymers demonstrated compressional elasticity increase in a linear fashion. Further compression at 34 $Å^2$ revealed a decrease in slope for both curves, indicating the formation of a more compact structure for both polymers, in which C-PLA displayed a lower compressional elasticity than that of L-PLA. As illustrated in Scheme 2, because of its confined structure and inherent absence of end groups and linear chains, C-PLA endures less interpenetration, leading to fewer entanglements and reptation during compression. At the plateau region (Figure S2), the elasticity of C-PLA drops to nearly zero, suggesting a first order transition, where the polymeric structure does not collapse but merely reorganizes.[14] After experiencing a sharp increase in the final compression region, the compressional modulus values drastically dropped upon reaching their highest limit. At this peak, the area per repeating unit is reported as a critical value, physically indicating the most possible compact structure of the floating film. Further compression at this point results in a collapsible film structure as illustrated by the compressional modulus drop. As shown in Figure 1b, the critical area per repeating unit for L-PLA and C-PLA are 6.5 and 4.1 $Å^2$, respectively, illustrating a more confined structure for the latter than the former.

Scheme 2

Isobaric Study. Isobaric creep experiments were performed to investigate the stability of the polymers over time, an essential property for a successful LB film preparation. The measurements were done under surface pressures of 4, 8, 15 mN m^{-1}, corresponding to three different isotherm regions, where each of these surface pressures was maintained constant, while monitoring the area change. In Figure 2, the time evolutional normalized area, A_t/A_0, is plotted against time, where A_t

is the area at any given time, t, and A_0 refers to the initial area. Compared to L-PLA, C-PLA exhibited slower decline in A_t/A_0 at 4 mN m^{-1}, with an area loss (i.e. <10%) lower than L-PLA (i.e. ~30%). This result, which suggests higher stability for C-PLA than L-PLA, may be due to the (i) more compact structure of C-PLA, resulting in a higher resistance against multilayer collapse, and (ii) absence of end groups, leading to a low hydrolysis rate[35] and minimal material loss at the interface. Exhibiting similar behavior at both 4 and 8 mN m^{-1}, the curve for L-PLA is characterized initially by a drastic area loss, followed by a nearly A_t/A_0 plateau beginning at 3000 s. In contrast, both C-PLA and DC-PLA showed a linear behavior characterized by a continuous but relatively slower decrease in rate of area loss. Meanwhile, Figure 2c, which displays the area loss at a surface pressure of 15 mN m^{-1}, reveals that the three polymers stabilize at a common area loss of roughly 12%. This result, which is in good agreement with a polylactide material reported in the literature[18] indicates that all the polymers are capable of rapidly attaining equilibrium at high surface pressures, with C-PLA film being the most stable as evidenced by its slower relaxation and lower area loss at 15 mN m^{-1}.

Figure 2

Hysteresis study. We also investigated the stability of the PLA monolayers using the results obtained from compression-expansion experiments. Figure 3 shows the compression-expansion cycles of L-PLA and DC-PLA at 4 and 8 mN m^{-1} and temperature of 20 °C. At low surface pressure of 4 mN m^{-1}, DC-PLA revealed a more improved reversibility, while L-PLA showed a more apparent hysteresis. C-PLA, on the other hand, showed a slight hysteresis (Figure S3), but much less than that of L-PLA. Again, DC-PLA's confined structure and absence of end groups result in less entanglement and reptation during compression, largely reducing its hysteresis phenomenon. Also, the L-PLA curves after each compression cycle slightly shifted to the smaller area. This

result may be caused by its adherence to the Wihelmy plate, desorption at the air-water interface, and entanglement irreversibility.[36] Meanwhile, the less area change for DC-PLA (Figure S3(b1)) is an indication of its more stable LB film formation than L-PLA. Likewise, less hysteresis and less area loss for DC-PLA than those of L-PLA were also observed at a higher surface pressure of 8 mN m^{-1}. Similar conclusions can also be drawn for C-PLA for its less hysteresis and less area loss (Figure S3). Furthermore, at a high surface pressure of 25 mN m^{-1} region, L-PLA, C-PLA, and DC-PLA showed significant decrease in their area (Figure S3) after the first compression-expansion cycle, indicating the irreversibility of their respective LB films at the air-water interface.

Figure 3

Deposited Film Study. To obtain an overview of the morphology and nanoscale structures of C-PLA and L-PLA, the corresponding LB films at different surface pressures were transferred to silica wafers for AFM study. Surface pressures of 4, 8, and 25 mN m^{-1}, representing the three different isotherm zones were chosen. As shown in Figure 4, a morphology difference between L-PLA and C-PLA at 4 mN m^{-1} can be observed. C-PLA showed a nanofiber-like morphology, with a height between 1 and 1.5 nm and width of 20 nm as determined by a higher resolution scan (Figure S4a). This structural morphology, caused by lamellar crystal formation, is a characteristic of polylactide and its stereocomplex,.[19] On the other hand, L-PLA revealed fewer and wider nanofiber-like structures with a flat morphology (Figure 4b and Figure S4b.) Again, the difference in morphology can be explained by their structural changes during isothermal compression. As previously shown in Scheme 2, L-PLA forms entanglements during compression, preventing crystal formation due to restricted chain mobility, while C-PLA becomes crystalline much easier due to its confined structure and less entanglements. This phenomenon can be evidenced by C-PLA's DSC curve in Figure S5, which shows lower glass transition temperature than L-PLA,

implying less chain movement hindrance. The lower melting temperature of C-PLA (144 °C) than L-PLA (166 °C), which is in good agreement with previously reported catenated polycaprolactone, also supports this hypothesis.[32] These results help explain why C-PLA requires a lower area per repeating unit to spread over the air-water interface and higher surface pressure in isotherms. As shown in Figure S5a, compared to L-PLA, C-PLA forms a smoother film structure with a thickness of 2 nm. By further compression to a surface pressure of 12 mN m^{-1}, nanofiber like structures can be observed on the morphology of L-PLA (Figure S7a), indicating a higher force requirement for polymer crystallization, while DC-PLA, at 8 mN m^{-1}, forms a structure similar to that of C-PLA (Figure S7b). At 25 mN m^{-1}, both L-PLA and C-PLA form collapsed multilayer but with different surface topology (Figure S8).

Figure 4

EIS, along with the use of an equivalent electrical circuit to fit the resulting impedance data, is a very useful electrochemical tool for the analysis of many polymeric coatings.[ref] We performed EIS to study the electrochemical surface behavior of our deposited L-PLA and C-PLA films on gold-coated glass slides at a surface pressure of 25 mN m^{-1}. The shape of the resulting Nyquist plots in Figure 5 is composed of a semicircle characterized by a solution resistance (R_s) in series with a parallel pair of double layer capacitance (C_{dl}) and charge transfer resistance (R_{ct}), followed by a low-frequency slanted line corresponding to a Warburg (Z_W) diffusional process. As shown by its larger semicircle diameter plot, C-PLA exhibits a larger R_{ct} value, indicating higher electron-transfer resistance (~90 Ω cm^2) at the interface than L-PLA (~19 Ω cm^2). This result is an indication of a lower C-PLA film conductivity than that of the L-PLA, which supports the deduction of a more compact structure of the former than the latter polymer.

Figure 5

XRR was performed to investigate the layered structure and interfacial properties of the polymer films deposited on a silicon wafer at 8 mN m^{-1}. The results acquired, together with the fitted data were plotted in Figure S9, while the XRR parameters extracted from the fitting are tabulated in Table 1. At 8 mN m^{-1} surface pressure, C-PLA film is composed of two layers – one exposed to air (layer 1), while the other adheres to the silicon wafer surface (layer 2). The total thickness of the C-PLA film is 2.2 nm, which is in good agreement with the result obtained from AFM experiments. The thickness and roughness values of each layer of the L-PLA film are nearly equal to those of C-PLA, but the scattering length density (SLD) of layer 2 of the latter is lower than the former. This difference in SLD result can be attributed to the different assembly process of both polymers. Note that the two polymer films were deposited at the same surface pressure of 8 mN m^{-1}, at which L-PLA displayed a much lower area per repeating unit based on the isotherm experiment. This result suggests that larger amounts of L-PLA were compressed to give a higher SLD for the whole film. In contrast, higher area per repeating unit means that less amounts of the polymer materials were compressed to form layer 2, as in the case of C-PLA. Based on the results obtained from AFM, the morphology showed a more compact film where C-PLA aggregated while its total SLD remained lower because of loosened spaces in the total film.

Table 1: Parameters extracted from XRR fitting.

Sample		Thickness (nm)	SLD(10^{-6} A^{-2})	Roughness(nm)
C-PLA	Layer 1	1.1	7.7	0.8
	Layer 2	1.1	15.6	0.6

L-PLA	Layer 1	1.0	7.3	0.8
	Layer 2	1.0	20.2	0.7

CONCLUSION

The interfacial behavior of catenated polymers at the air-water interface was investigated, where C-PLA and DC-PLA, in comparison to L-PLA, demonstrated unique and distinctive interfacial properties as evidenced by surface pressure-area per repeating unit isotherms. Isobaric creep and compression-expansion cycles revealed that C-PLA and DC-PLA are highly stable at the air-water interface. In addition, polymer films at different surface pressures were transferred to silica wafers via LB method to observe their surface morphology. C-PLA showed nanofiber-like structures at low surface pressure, but formed a more compact film at high surface pressure than L-PLA. This result is supported by the impedance measurement, where a higher R_{ct} value for C-PLA than L-PLA was obtained. Overall, our initial assessment on the interfacial behavior of C-PLA at the air-water interface will pave the way for more detailed surface characterization study for topological polymers.

FIGURES

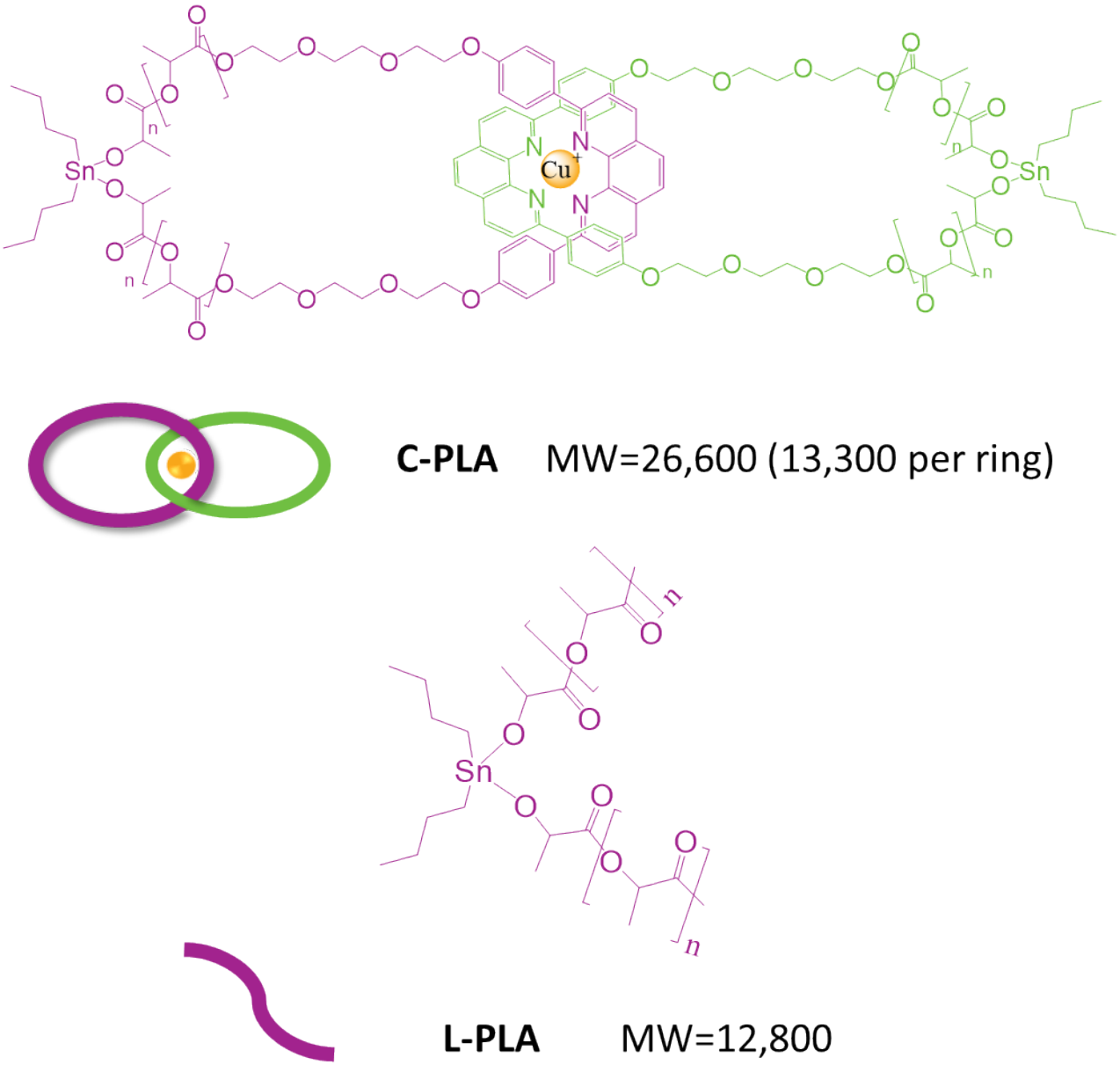

Scheme 1: Chemical structures of C-PLA and L-PLA. For comparison, the molecular weight of each ring in C-PLA is designed to be nearly equal to L-PLA.

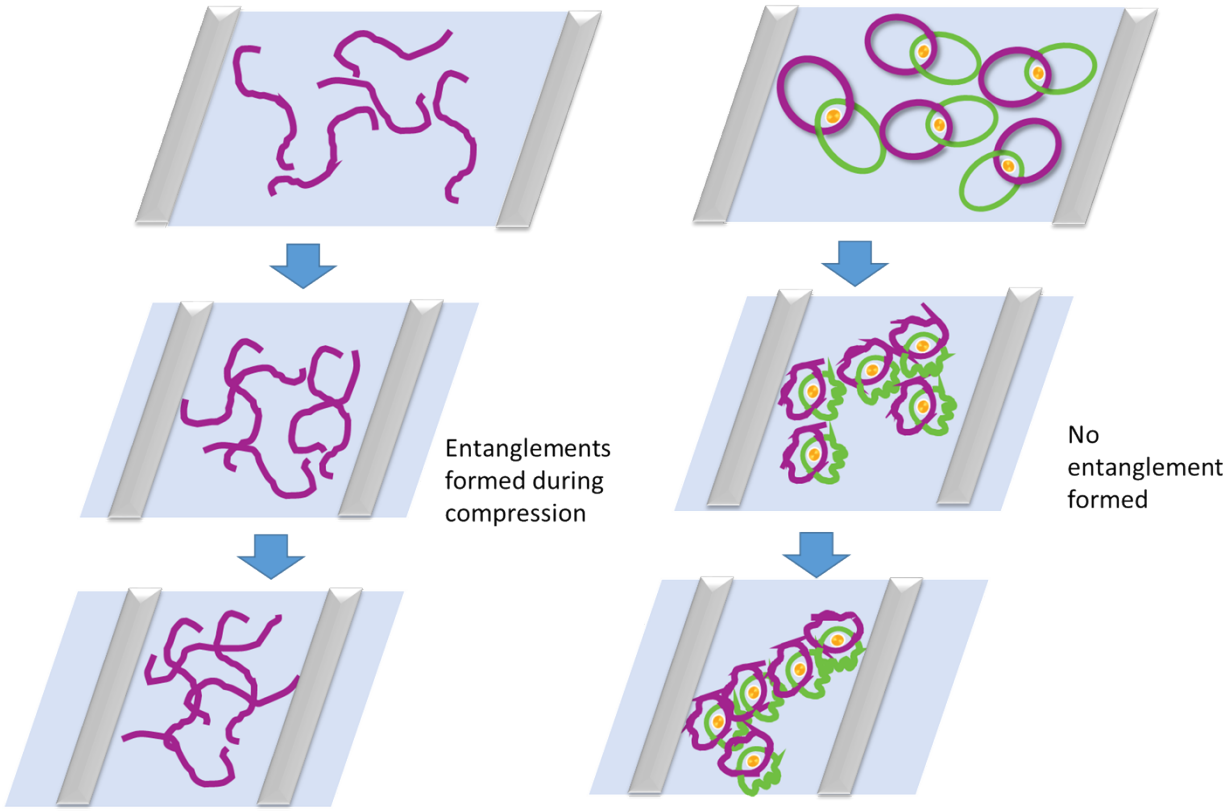

Scheme 2: Schematic representation of structural changes of the polymers during compression.

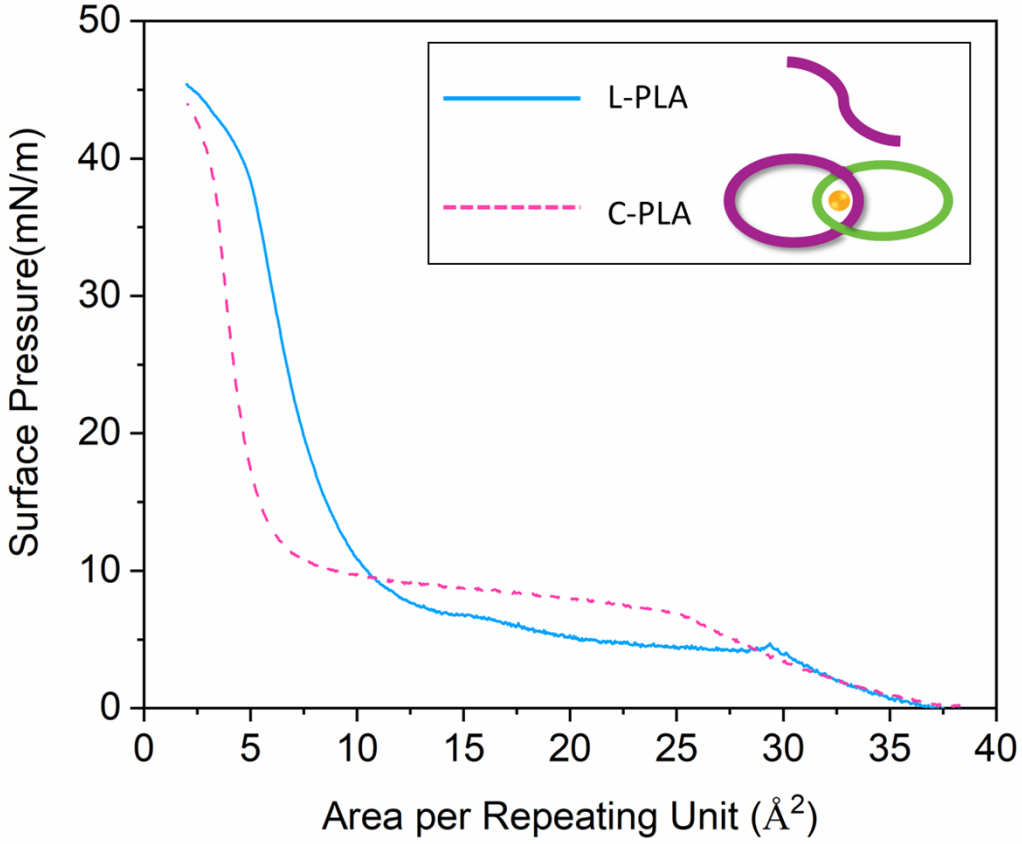

Figure 1: Isothermal π-A compression curves for L-PLA and C-PLA.

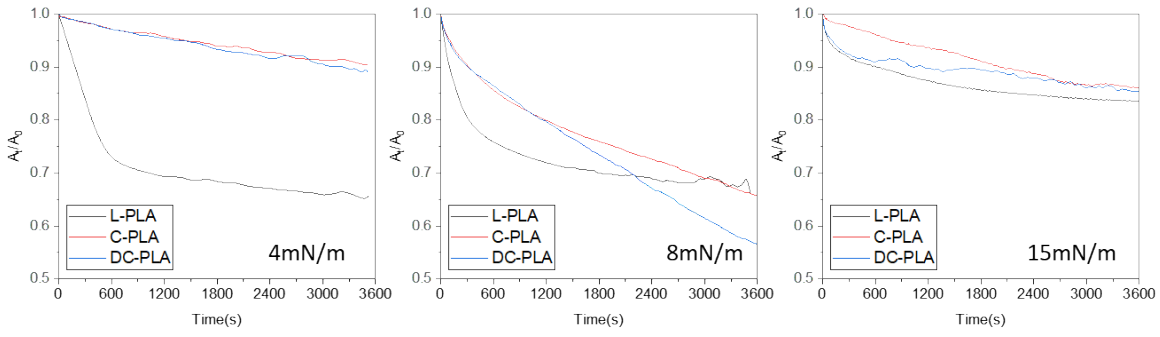

Figure 2: A_t/A_0 vs. time curves obtained from isobaric creep measurements at 4, 8, 15 mN/m

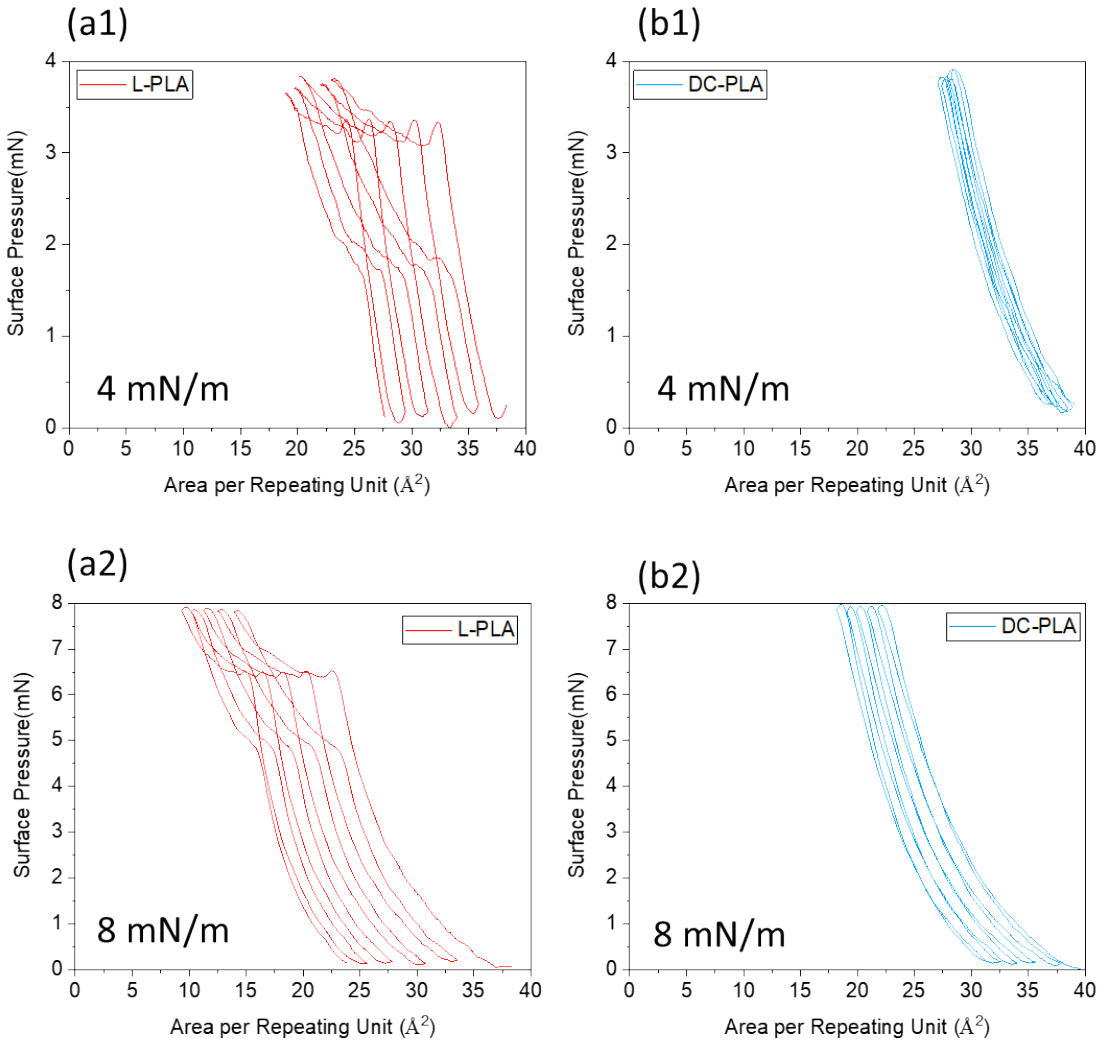

Figure 3: Compression-expansion curves for L-PLA and DC-PLA at 4 and 8 mN/m.

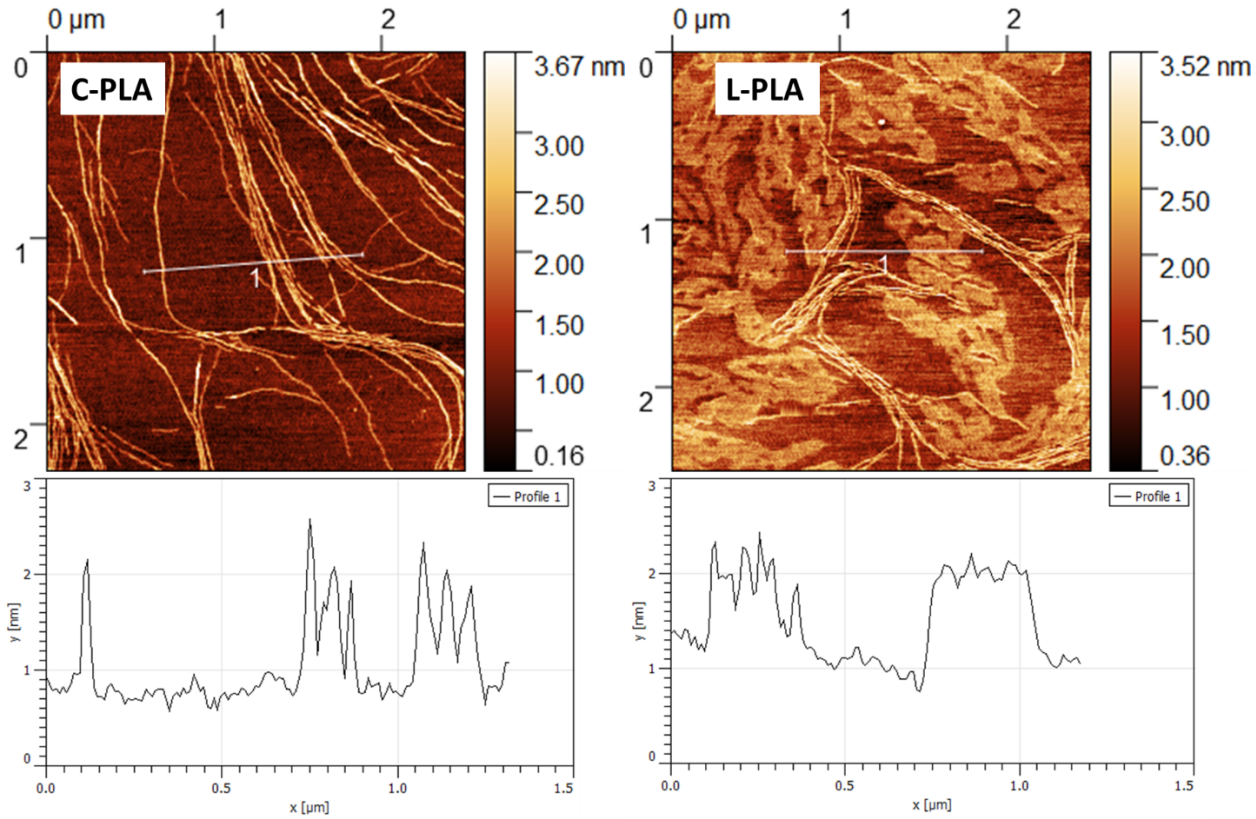

Figure 4: AFM scan of C-PLA and L-PLA deposited on silica wafer at 4 mN/m.

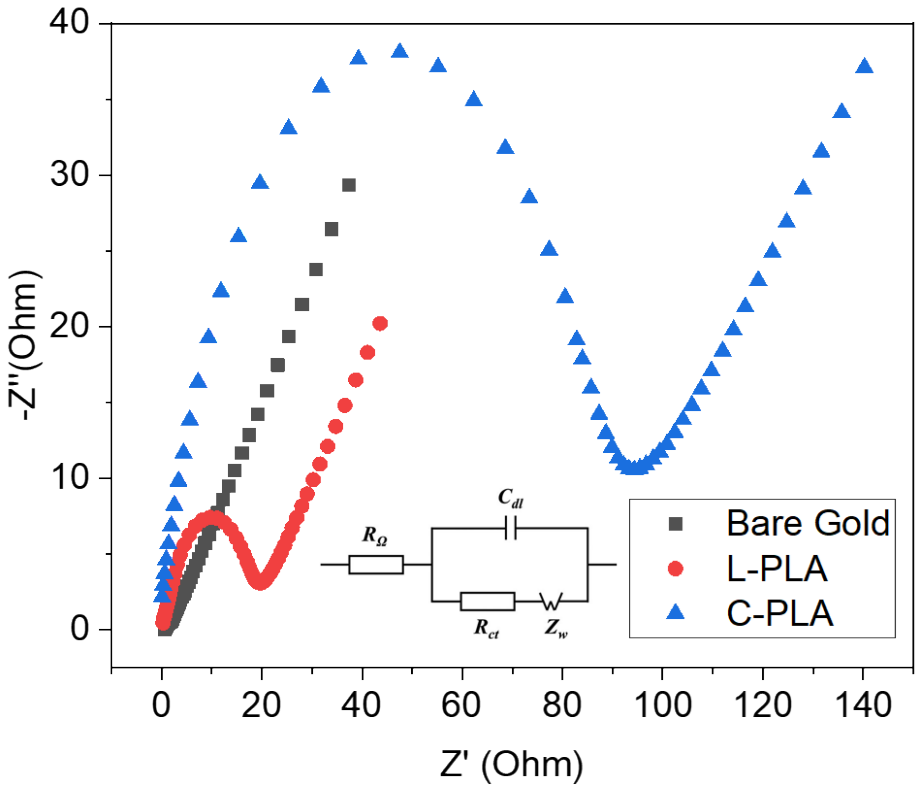

Figure 5: Nyquist diagrams for bare gold, L-PLA, and C-PLA, and the corresponding equivalent electrical circuit model.

ASSOCIATED CONTENT

Supporting Information.

The Supporting Information is available free of charge on the ACS Publications website.

Detailed information on the preparation and characterization of different core-shell nanomaterials and corresponding films (PDF)

AUTHOR INFORMATION

Corresponding Author

*Email: caop@ornl.gov.

*Email: rca41@case.edu.

ORCID

Li-Han Rong: 0000-0002-9351-059X

Xiang Cheng: 0000-0002-3308-3506

Jin Ge:

Hanyu Wang:

Peng-Fei Cao: 0000-0003-2391-1838

Eugene B. Caldona:

Rigoberto C. Advincula: 0000-0002-2899-4778

Author Contributions

The manuscript was written through contributions of all authors. All authors have given approval to the final version of the manuscript.

Notes

The authors declare no competing financial interest.

REFERENCES

1. Zhao, L.; Lin, Z., Self-assembly of non-linear polymers at the air/water interface: the effect of molecular architecture. *Soft Matter* **2011,** *7* (22), 10520-10535.

2. Logan, J. L.; Masse, P.; Gnanou, Y.; Taton, D.; Duran, R. S., Polystyrene-block-Poly(ethylene oxide) Stars as Surface Films at the Air/Water Interface. *Langmuir* **2005,** *21* (16), 7380-7389.

3. Honda, S.; Yamamoto, T.; Tezuka, Y., Tuneable enhancement of the salt and thermal stability of polymeric micelles by cyclized amphiphiles. *Nature Communications* **2013,** *4* (1), 1574.

4. Li, Z.; Ma, X.; Zang, D.; Guan, X.; Zhu, L.; Liu, J.; Chen, F., Interfacial rheology and aggregation behaviour of amphiphilic CBABC-type pentablock copolymers at the air–water interface: effects of block ratio and chain length. *RSC Advances* **2015,** *5* (101), 82869-82878.

5. Xu, W.; Ledin, P. A.; Iatridi, Z.; Tsitsilianis, C.; Tsukruk, V. V., Multiresponsive Star-Graft Quarterpolymer Monolayers. *Macromolecules* **2015,** *48* (10), 3344-3353.

6. Ariga, K., Don't Forget Langmuir–Blodgett Films 2020: Interfacial Nanoarchitectonics with Molecules, Materials, and Living Objects. *Langmuir* **2020,** *36* (26), 7158-7180.

7. McCullough, I. I. I. D. H.; Regen, S. L., Don't forget Langmuir–Blodgett films. *Chemical Communications* **2004,** (24), 2787-2791.

8. Ji, W.; Zhao, W.; Li, W.; Wang, Y.; Wang, J.; Lan, D., Hydrodynamic Process in the Langmuir-Blodgett Film Method. *Langmuir* **2020,** *36* (47), 14461-14469.

9. Gabaji, M.; Médard, J.; Hemmerle, A.; Pinson, J.; Michel, J. P., From Langmuir–Blodgett to Grafted Films. *Langmuir* **2020,** *36* (10), 2534-2542.

10. Wu, J.; Lieser, G.; Wegner, G., Direct imaging of individual shape-persistent macromolecules and their interaction by TEM. *Advanced Materials* **1996,** *8* (2), 151-154.

11. Frey, W.; Schief, W. R.; Vogel, V., Two-Dimensional Crystallization of Streptavidin Studied by Quantitative Brewster Angle Microscopy. *Langmuir* **1996,** *12* (5), 1312-1320.

12. Qiu, Y.; Chen, P.; Liu, M., Evolution of Various Porphyrin Nanostructures via an Oil/Aqueous Medium: Controlled Self-Assembly, Further Organization, and Supramolecular Chirality. *Journal of the American Chemical Society* **2010,** *132* (28), 9644-9652.

13. Wang, X.-L.; Wang, Y.-L.; Miao, W.-K.; Hu, M.-B.; Tang, J.; Yu, W.; Hou, Z.-Y.; Zheng, P.; Wang, W., Langmuir and Langmuir–Blodgett Films of Hybrid Amphiphiles with a Polyoxometalate Headgroup. *Langmuir* **2013,** *29* (22), 6537-6545.

14. Scherz, L. F.; Schroyen, B.; Pepicelli, M.; Schlüter, D. A.; Vermant, J.; Vlassopoulos, D., Molecularly Designed Interfacial Viscoelasticity by Dendronized Polymers: From Flexible Macromolecules to Colloidal Objects. *ACS Nano* **2019,** *13* (12), 14217-14229.

15. Scheibe, P.; Barz, M.; Hemmelmann, M.; Zentel, R., Langmuir−Blodgett Films of Biocompatible Poly(HPMA)-block-poly(lauryl methacrylate) and Poly(HPMA)-random-poly(lauryl methacrylate): Influence of Polymer Structure on Membrane Formation and Stability. *Langmuir* **2010,** *26* (8), 5661-5669.

16. Ha, C.-S.; Gardella, J. A., Surface Chemistry of Biodegradable Polymers for Drug Delivery Systems. *Chemical Reviews* **2005,** *105* (11), 4205-4232.

17. Liu, S.; Qin, S.; He, M.; Zhou, D.; Qin, Q.; Wang, H., Current applications of poly(lactic acid) composites in tissue engineering and drug delivery. *Composites Part B: Engineering* **2020,** *199*, 108238.

18. Klass, J. M.; Lennox, R. B.; Brown, G. R.; Bourque, H.; Pézolet, M., Enantiomeric Polylactides at the Air−Water Interface: π−A Isotherms and PM-IRRAS Studies of Enantiomers and Their Blend. *Langmuir* **2003,** *19* (2), 333-340.

19. Watanabe, K.; Kumaki, J., Extended-chain crystallization and stereocomplex formation of polylactides in a Langmuir monolayer. *Polymer Journal* **2020,** *52* (6), 601-613.

20. Iwashima, K.; Yamamoto, T.; Tezuka, Y.; Kumaki, J., Self-Assembly of Linear and Cyclic Polylactide Stereoblock Copolymers with a Parallel and Antiparallel Chain Arrangement Distinguishing Their Directions on a Water Surface. *Langmuir* **2020,** *36* (22), 6216-6221.

21. Gunawidjaja, R.; Peleshanko, S.; Genson, K. L.; Tsitsilianis, C.; Tsukruk, V. V., Surface Morphologies of Langmuir−Blodgett Monolayers of PEOnPSn Multiarm Star Copolymers. *Langmuir* **2006,** *22* (14), 6168-6176.

22. Su, A.; Tan, S.; Thapa, P.; Flanders, B. N.; Ford, W. T., Highly Ordered Langmuir−Blodgett Films of Amphiphilic Poly(propylene imine) Dendrimers. *The Journal of Physical Chemistry C* **2007,** *111* (12), 4695-4701.

23. Peleshanko, S.; Gunawidjaja, R.; Jeong, J.; Shevchenko, V. V.; Tsukruk, V. V., Surface Behavior of Amphiphilic Heteroarm Star-Block Copolymers with Asymmetric Architecture. *Langmuir* **2004,** *20* (22), 9423-9427.

24. Suntivich, R.; Choi, I.; Gupta, M. K.; Tsitsilianis, C.; Tsukruk, V. V., Gold Nanoparticles Grown on Star-Shaped Block Copolymer Monolayers. *Langmuir* **2011,** *27* (17), 10730-10738.

25. Fujii, S.; Morita, T.; Kimura, S., Fabrication of Langmuir–Blodgett Film of a Fullerene Derivative with a Cyclic Peptide as an Anchor. *Bioconjugate Chemistry* **2007,** *18* (6), 1855-1859.

26. Meng, Q.; Honda, S.; Tezuka, Y.; Yamamoto, T.; Fujimori, A., Topological “interfacial” polymer chemistry: Dependency of polymer “shape” on surface morphology and stability of layer structures when heating organized molecular films of cyclic and linear block copolymers of n-butyl acrylate-ethylene oxide. *Journal of Polymer Science Part B: Polymer Physics* **2016,** *54* (4), 486-498.

27. Adachi, J.; Mori, T.; Inoue, R.; Naito, M.; Le, N. H.-T.; Kawamorita, S.; Hill, J. P.; Naota, T.; Ariga, K., Emission Control by Molecular Manipulation of Double-Paddled Binuclear PtII Complexes at the Air-Water Interface. *Chemistry – An Asian Journal* **2020,** *15* (3), 406-414.

28. Brown, C. L.; Jonas, U.; Preece, J. A.; Ringsdorf, H.; Seitz, M.; Stoddart, J. F., Introduction of [2]Catenanes into Langmuir Films and Langmuir−Blodgett Multilayers. A Possible Strategy for Molecular Information Storage Materials. *Langmuir* **2000,** *16* (4), 1924-1930.

29. Jang, S. S.; Jang, Y. H.; Kim, Y.-H.; Goddard, W. A.; Choi, J. W.; Heath, J. R.; Laursen, B. W.; Flood, A. H.; Stoddart, J. F.; Nørgaard, K.; Bjørnholm, T., Molecular Dynamics Simulation of Amphiphilic Bistable [2]Rotaxane Langmuir Monolayers at the Air/Water Interface. *Journal of the American Chemical Society* **2005,** *127* (42), 14804-14816.

30. Bunha, A. K.; Mangadlao, J.; Felipe, M. J.; Pangilinan, K.; Advincula, R., Catenated PS-PMMA block copolymers via supramolecularly templated ATRP initiator approach. *Macromolecular rapid communications* **2012,** *33* (14), 1214-9.

31. Gan, Y.; Dong, D.; Hogen-Esch, T. E., Synthesis and Characterization of a Catenated Polystyrene−Poly(2-vinylpyridine) Block Copolymer. *Macromolecules* **2002,** *35* (18), 6799-6803.

32. Cao, P.-F.; Mangadlao, J. D.; de Leon, A.; Su, Z.; Advincula, R. C., Catenated Poly(ε-caprolactone) and Poly(l-lactide) via Ring-Expansion Strategy. *Macromolecules* **2015,** *48* (12), 3825-3833.

33. Cao, P.-F.; Bunha, A.; Mangadlao, J.; Felipe, M. J.; Mongcopa, K. I.; Advincula, R., A supramolecularly templated catenane initiator and a controlled ring expansion strategy. *Chemical Communications* **2012,** *48* (99), 12094-12096.

34. Ni, S.; Lee, W.; Li, B.; Esker, A. R., Thermodynamics of the Liquid Expanded to Condensed Phase Transition of Poly(l-lactic acid) in Langmuir Monolayers. *Langmuir* **2006,** *22* (8), 3672-3677.

35. Hoskins, J. N.; Grayson, S. M., Synthesis and Degradation Behavior of Cyclic Poly(ε-caprolactone). *Macromolecules* **2009,** *42* (17), 6406-6413.

36. Felipe, M. J.; Estillore, N.; Pernites, R. B.; Nguyen, T.; Ponnapati, R.; Advincula, R. C., Interfacial Behavior of OEG–Linear Dendron Monolayers: Aggregation, Nanostructuring, and Electropolymerizability. *Langmuir* **2011,** *27* (15), 9327-9336.

Table of Contents graphic